RESEARCH ARTICLE

Parametric equations for notch stress concentration factors of rib–deck welds under bending loading

Qiudong WANG, Bohai JI*, Zhongqiu FU, Yue YAO

College of Civil and Transportation Engineering, Hohai University, Nanjing 210098, China
*Corresponding author. E-mail: bhji@hhu.edu.cn

ABSTRACT   The effective notch stress approach for evaluating the fatigue strength of rib–deck welds requires notch stress concentration factors obtained from complex finite element analysis. To improve the efficiency of the approach, the notch stress concentration factors for three typical fatigue-cracking modes (i.e., root–toe, root–deck, and toe–deck cracking modes) were thoroughly investigated in this study. First, we developed a model for investigating the effective notch stress in rib–deck welds. Then, we performed a parametric analysis to investigate the effects of multiple geometric parameters of a rib–deck weld on the notch stress concentration factors. On this basis, the multiple linear stepwise regression analysis was performed to obtain the optimal regression functions for predicting the notch stress concentration factors. Finally, we employed the proposed formulas in a case study. The notch stress concentration factors estimated from the developed formulas show agree well with the finite element analysis results. The results of the case study demonstrate the feasibility and reliability of the proposed formulas. It also shows that the fatigue design curve of FAT225 seems to be conservative for evaluating the fatigue strength of rib–deck welds.

KEYWORDS   notch stress concentration factor, rib–deck weld, parametric analysis, regression analysis, parametric equation

1   Introduction

Rib–deck welds are one of the most fatigable details in orthotropic steel decks (OSDs). Fatigue assessment of rib–deck welds has raised great concern recently [1–6]. Several stress-based approaches, such as the nominal stress, hot-spot stress, and effective notch stress approaches, could be employed in the fatigue assessment of rib–deck welds [7]. Among them, the nominal stress approach is the simplest. In this approach, fatigue assessment is performed using specific S–N curves corresponding to the structural details. However, the structure-related stress concentration is not included in the approach, which could lead to inaccurate evaluation results. The hot-spot stress method has higher accuracy than the nominal stress method because it considers the effect of the structural configuration (i.e., the structure-related stress concentration). However, the notch stress induced by weld beads cannot be determined by the hot-spot stress approach due to the limitation of stress extrapolation, as shown in Fig. 1. Additionally, the

hot-spot stress approach is not applicable to the weld roots of rib–deck welds where most fatigue cracks initiate [7]. Alternatively, the effective notch stress approach, which has an increased precision by considering the nonlinear peak induced by the presence of the weld, could precisely account for the notch stress. Therefore, the effective notch stress approach has a broad application prospect in structural engineering.

The concept of the effective notch stress approach was conceived by Radaj [8] when he derived a fictitious rounding of a notch stress model of welds based on Neuber's assumptions [9]. Köttgen et al. [10] further developed the effective notch stress approach, as embedded in the IIW recommendations [7]. To employ the effective notch stress approach, a stress concentration factor (K_t) is required. K_t could be obtained by replacing the actual weld contour with a fictitious round notch. For most structural components with plate thickness greater than 5 mm, an effective notch radius of $r = 1$ mm is usually recommended [7]. In this case, K_t could also be intrinsically interpreted as the effective notch stress concentration factor (K_f). K_f is key in the application of

the effective notch stress approach. Once K_f is obtained, the effective notch stress (σ_{en}) could be determined by multiplying the nominal stress (σ_n) by K_f.
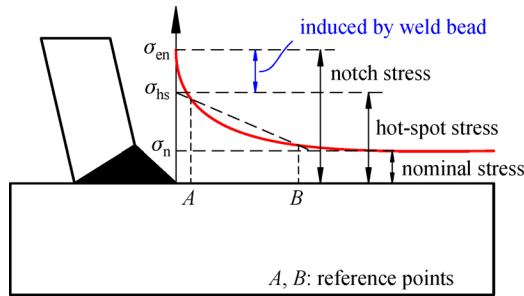

Fig. 1   Fatigue stress at a weld.

K_f could be obtained by numerical simulations, such as finite element analysis (FEA). This process requires the development of a finite element model introduced by an effective notch at weld toe or root and sensitivity analysis of the meshing size to obtain reliable and numerically good-quality results [11]. Such requirement prevents many engineers from employing the effective notch stress approach in fatigue assessment of welded joints. As an alternative to the complex and time-consuming numerical simulations, empirical formulas obtained from regression analysis are a better choice for determining K_f. If such formulas provide high-accuracy results, their application would save time, effort, and cost. For this reason, several efforts have been made to develop empirical formulas for K_f in simple connections, such as welded cruciform joints [12–14], T-butt welded connections [15,16], and butt welds [17]. Recently, studies on the application of the effective notch stress approach on rib–deck welds have been reported [6,18–20]. However, only a few studies have focused on the empirical formula for K_f. Therefore, there is a need to develop the empirical formulas for K_f in rib–deck welds to enhance the efficient use of the effective notch stress approach.

In this study, finite element models (FEMs) that simulate rib–deck welded structures were developed and validated. Parametric analysis was performed to investigate the effect of weld geometric parameters on K_f. On this basis, regression analysis was performed to obtain the empirical formula for K_f. Finally, a case study was presented to

investigate the application of the proposed formulas in the fatigue assessment of rib–deck welded specimens.

2   Finite element modeling

2.1   Model

FEA was performed to obtain K_f in the weld toe and root of a rib–deck weld. Figure 2 shows the schematic diagram of the model. The model has a transverse width of $3 \times W_d$ and a longitudinal length of L_d. In this study, W_d and L_d were set to 300 and 100 mm, respectively. The height of the U-rib was 240 mm. Since this study was focused on local parameters (i.e., K_f at the weld toe and root), the dimensions were large enough for the effect of boundary conditions to be neglected, according to Saint Venant's principle [21]. The geometric parameters of the rib–deck welded joint are depicted in Fig. 2, showing the deck thickness (t_d), rib thickness (t_r), weld penetration rate ($1 - t_p/t_r$), weld leg length in the deck ($l_{w,d}$), weld leg length in the rib ($l_{w,r}$), and the angle between the deck and rib (θ). The geometric parameters of the rib–deck weld were assigned different values for the parametric analysis, as discussed in Section 4.

To obtain K_f at the weld toe and root, a round notch with a radius of 1 mm was introduced according to the IIW recommendations [7]. All models were simulated by SOLID186-type elements in ANSYS. This element is defined by 20 nodes having three degrees of freedom each; translations in the nodal x, y, and z directions. The element supports plasticity, hyper-elasticity, creep, stress-stiffening, large deflection, and large strain capabilities. To obtain K_f, an elastic analysis was performed by setting the Young modulus (E) and Poisson ratio (v) of the steel material to 206 GPa and 0.3, respectively. For the boundary conditions, both ends of the deck plate in the transverse direction were fixed. That is, for the nodes at the two ends of the deck plate, displacements along x, y, and z directions were fixed. Surface loads of magnitude 1.0 MPa were applied at both sides of the U-rib, $W_d/2$ away from the end of the deck plate. In this case, the objective rib–deck weld was subjected to pure bending loading. The developed FEMs built are shown in Fig. 3. The meshing of the FEMs is detailed in Section 2.2.
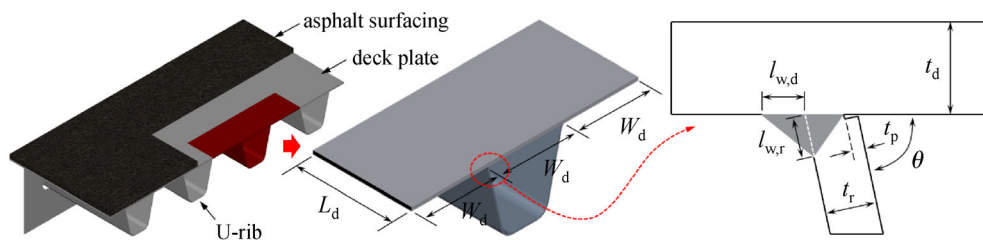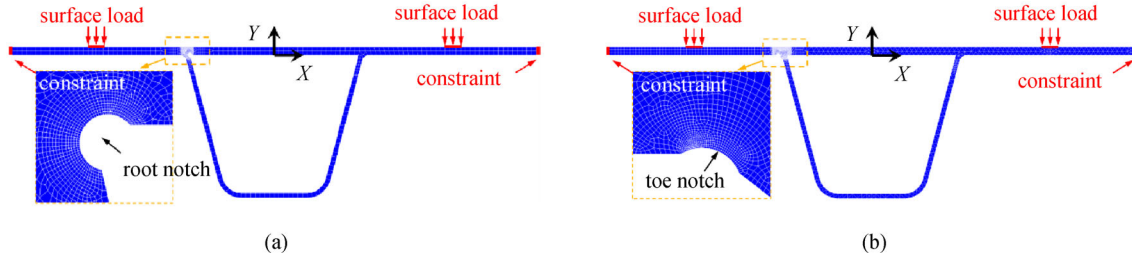

Fig. 2   Schematic of the model.

Fig. 3 Finite element models with weld root or toe notch under bending loading. (a) Weld root notch; (b) weld toe notch.

Steel is usually a strain-hardening material with a specific constitutive relationship. However, to obtain K_f at the introduced notch, an elastic analysis is considered, as recommended by IIW [7]. Thus, in this study, the steel material was simply assigned a linear elastic constitutive relation.

2.2 Effect of meshing size

Effective notch stress is sensitive to the size of the element around the notch. For a 20-node SOLID186-type element-simulated model, the number of elements in 360° arc is recommended to be at least 24 [7]. Thus, the number of elements in 282° arc (i.e., corresponding to θ of 78°) should be at least 18.8. To further determine the suitable number of elements for rib–deck welds, the effective notch stresses in the weld root of a fully penetrated rib–deck weld were extracted for sensitivity analysis. The number of elements at the notch edge was set to 5, 10, 20, 30, and 40, respectively. To improve the calculation accuracy and decrease the computational cost, the meshing transition region was arranged near the notch, as illustrated in Ref. [19]. The coarse meshing size was set to 6 mm.

Considering that the stress distribution at the middle part of the FEM was less affected by the boundary conditions, the stresses thereat were extracted for investigation. The maximum stress perpendicular to the weld (σ_x), the first principal stress (σ_1), and von Mises equivalent stress (σ_s) around the notch are plotted in Fig. 4. The stresses first decrease and then remain stable as the meshing size increases. When the number of elements at the notch edge exceeds 20, the stresses become constant with the meshing size. This indicates that the number of elements must not be less than 20 in a 282° arc (i.e., 26 in 360° arc). Therefore, the number of elements in 360° arcs was taken as 30 in this study. The meshing size was precise enough for determining K_f.

2.3 Definition of the notch stress concentration factor

To determine K_f, it is essential to obtain the nominal stress at the weld toe or root first, as expressed in Eq. (1). Figure 5 shows the distribution of the stress component σ_x. There is a severe stress concentration at both the weld toe and root.
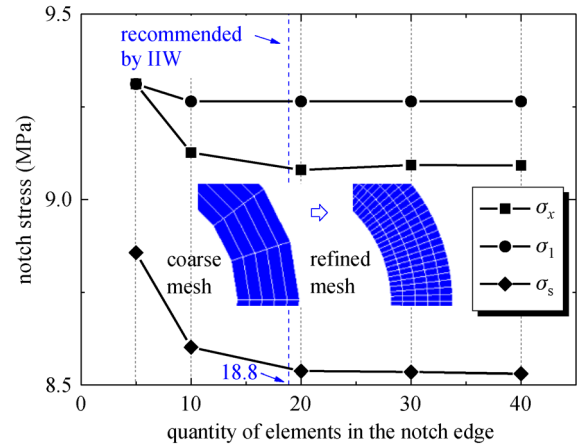

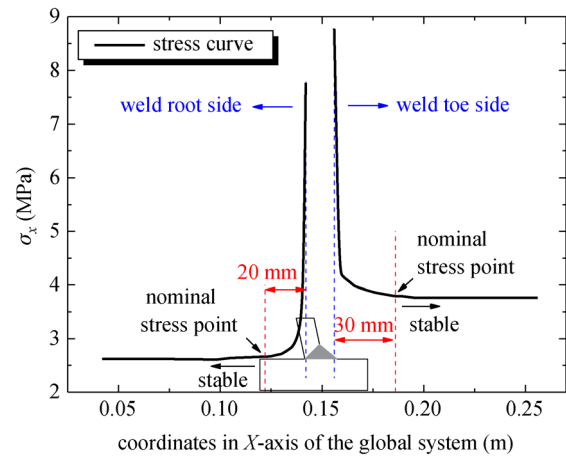**Fig. 4** Effect of meshing size on the effective notch stress.

Fig. 5 Determination of the nominal stress points.

The stress decreases sharply first and then remains stable as the extraction point moves away from the weld toe or root. For rib–deck welds, the extracting point 20 mm away from the weld root or 30 mm from the weld toe could be regarded as the nominal stress point.

Furthermore, effective notch stress could be determined by different stresses (σ_x, σ_1, or σ_s), which could affect the calculated K_f. To investigate such effects, taking the fully

penetrated rib–deck weld as an example, the values of K_f determined by different stresses are plotted in Fig. 6. K_f corresponding to σ_1 is close to that corresponding to σ_s. It reveals that K_f could be determined by either σ_1 or σ_s. In this study, σ_s was used to determine K_f.

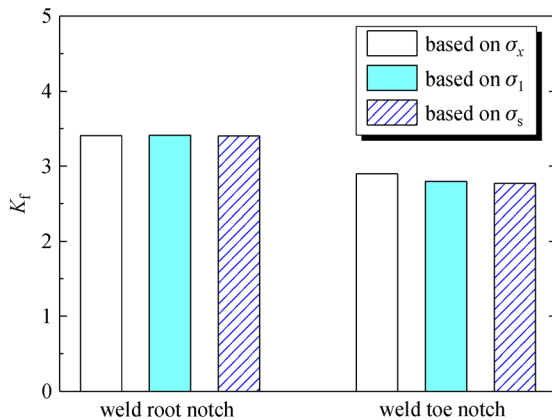$$K_f = \sigma_{en}/\sigma_n. \qquad (1)$$

Fig. 6 K_f based on different stresses.

3 Validation of the model

As mentioned earlier, a few empirical formulas for the K_f of rib–deck welds have been reported. Hence, we referred to the empirical formula for the K_f of a cruciform joint proposed by Oswald et al. [11] to validate the accuracy of the model for determining K_f. The estimation results were compared to those of the FEA using the same method discussed in Section 2.

Considering the full penetrated cruciform joint (Fig. 7), K_f at the weld toe could be predicted using Eq. (2). For comparison, a FEM for simulating cruciform joints was also developed using the same method discussed in Section 2 (Fig. 8). A round notch with a radius of 1 mm was set at the weld toe. Symmetric boundary conditions were employed to improve the computing accuracy, as marked in Fig. 8. A 0.5 MPa tensile load was then applied to the FEM for elastic analysis.

$$K_f = \sum_{k=1}^{10} c_k \cdot f_k(\alpha, t_1, y), \qquad (2)$$

where α is the flank angle, t_1 the plate thickness, $y = l_1/t_1$, l_1 the weld leg lengths, f_k the variables, c_k the coefficients, and subscript k the sequence number of each term. Since there are 10 terms in Eq. (2), k ranges from 1 to 10. The values of c_k are listed in Table 1. Both estimated and numerical results are plotted in Fig. 9. The numerical results are consistent with the estimated ones (i.e., calculated by Eq. (2)). The maximum error of the estimated results relative to the numerical results is within 1%, demonstrating the feasibility and reliability of the model in determining K_f.

4 Parametric analysis

4.1 Objective stress concentration positions

Extensive studies have been conducted to investigate the fatigue performance of rib–deck welds [1–3,5,6,22,23]. Through experimental investigations, three typical fatigue cracks are observed in rib–deck welds: (1) the root–toe crack (Fig. 10(a)); (2) the root–deck crack (Fig. 10(b)); and (3) the toe–deck crack (Fig. 10(c)). In a previous study [19], the feasibility of predicting the crack initiation position through the effective notch stress approach was preliminarily validated. In this study, FEMs for simulating the tested specimens in Refs. [2,3] were developed. The corresponding stress nephogram around the notch is depicted in Fig. 10. The crack initiation positions determined by FEA are similar to those determined by experiments. For example, considering 15% penetrated specimens (Fig. 10(a)), the stress concentration position at the notch edge (i.e., CP1) is consistent with the initiation position of the root–toe crack. Hence, in this study, K_f in all possible crack initiation positions (i.e., CP1 for root–toe crack, CP2 for root–deck crack, and CP3 for toe–deck crack) are investigated.

4.2 Parametric analysis

As shown in Fig. 2, the geometry of a rib–deck weld is determined using deck thickness (t_d), rib thickness (t_r), weld penetration rate ($1 - t_p/t_r$), weld leg length in the deck ($l_{w,d}$), weld leg length in the rib ($l_{w,r}$), and angle between the deck and rib (θ). We investigated multiple geometric parameters using the developed FEMs. The relative deck thickness (t_d/t_r) corresponding to a rib thickness of 6 mm

Table 1 Coefficients of the regression formula for K_f of full penetrated cruciform joints

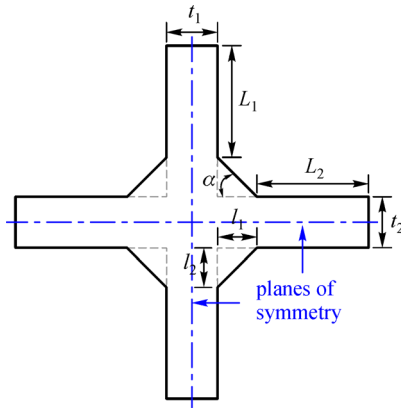| k	f_k	c_k	k	f_k	c_k	k	f_k	c_k
1	1	0.07171	5	α^2	− 0.00072	9	$t_1 y$	0.00432
2	α	0.07442	6	t_1^2	− 0.00026	10	αy	0.00892
3	t_1	0.02698	7	y^2	− 0.16891	–	–	–
4	y	− 0.06121	8	$t_1 \alpha$	0.00049	–	–	–

Fig. 7 Geometry of a full penetrated cruciform joint. Herein, $t_1 = t_2 = 20$ mm, $L_1 = L_2 = 40$ mm, $l_1 = l_2 = 10$ mm, $\alpha = 45°$.

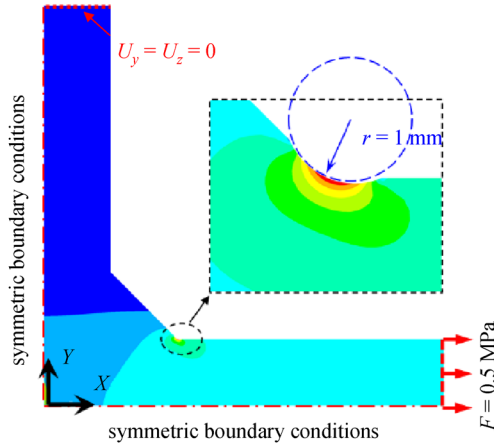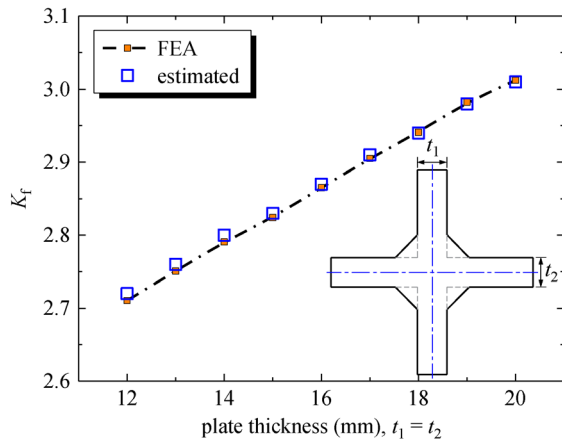**Fig. 8** Nephogram of the first principle stress, including the boundary conditions.

Fig. 9 Comparison of the FEA and estimated results. $L_1 = L_2 = 40$ mm, $l_1 = l_2 = 10$ mm, $\alpha = 45°$.

was set to 1.8, 2.0, and 2.5 to investigate the effect of deck thickness on K_f. The rib thickness (t_r) was set to 6, 8, and 10 mm to investigate the effect of rib thickness. The weld penetration rate ($1 - t_p/t_r$) was increased from 0 to 0.8 at a 0.1 interval. The relative weld leg length in the deck ($l_{w,d}/t_r$) and that in the rib ($l_{w,r}/t_r$) was increased from 0.8 to 1.2 at a 0.2 interval. Furthermore, θ was increased from 70° to 80° at a 5° interval. K_f in CP1, CP2, and CP3 were determined using Eq. (1), and the results are plotted in Figs. 11–13, respectively. In light of the purpose of this study, other quantitative results are not presented; however, they are available with the authors if required.

Figure 11 shows the variation of K_f in CP1. It decreases with an increase in the weld penetration rate ($1 - t_p/t_r$) but increases with the rib thickness (Fig. 11(a)). It decreases with an increase in $l_{w,d}/t_r$ and $l_{w,r}/t_r$, θ, and t_d/t_r. It varies more with $l_{w,r}/t_r$ and t_d/t_r (Figs. 11(c) and 11(e)) and less with the other geometric parameters (Figs. 11(a), 11(b), and 11(d)). This shows that increasing t_d or $l_{w,r}$ is more beneficial than increasing $l_{w,d}$, t_r and θ for reducing the stress concentration in CP1.

Figure 12 shows the variation of K_f in CP2. In general, K_f in CP2 increases with the weld penetration rate ($1 - t_p/t_r$). It decreases with an increase in t_r at small weld penetration rates (less than 40%) and remains unchanged at large weld penetration rates. As shown in Figs. 12(b) and 12(d), K_f in CP2 increases with $l_{w,d}/t_r$ and θ, but it remains constant at $l_{w,r}/t_r$ less than 1.0, as shown in Fig. 12(c). At $l_{w,r}/t_r$ greater than 1.0, a slight decrease in K_f is observed. K_f decreases with an increase in t_d/t_r, as shown in Fig. 12(e).

Figure 13 shows the variation of K_f in CP3, i.e., in the weld toe. K_f is independent of the weld penetration rate ($1 - t_p/t_r$). It is also considered independent of θ and t_d/t_r, as shown in Figs. 13(d) and 13(e), respectively. As shown in Figs. 13(a)–13(c), K_f increases with t_r and $l_{w,r}/t_r$ but decreases with increase in $l_{w,d}/t_r$. However, the effect of $l_{w,d}/t_r$ and $l_{w,r}/t_r$ is not obvious.

The observations from Figs. 11–13 reveal the significant effect of the geometric parameters of rib–deck welds on K_f. To develop empirical formulas for K_f, the coupled effects of different parameters should be reasonably considered.

5 Regression analysis

5.1 Regression formula for effective notch stress concentration factor

Based on the parametric analysis results, multi-parameter regression analysis was performed to develop the formulas for K_f in rib–deck welds (i.e., CP1, CP2, and CP3). The parametric analysis results show that the relationship between the geometric parameters and K_f is fitted with the linear fitting curve. In addition, since six variables may be related to K_f, it is essential to find the best-fitting
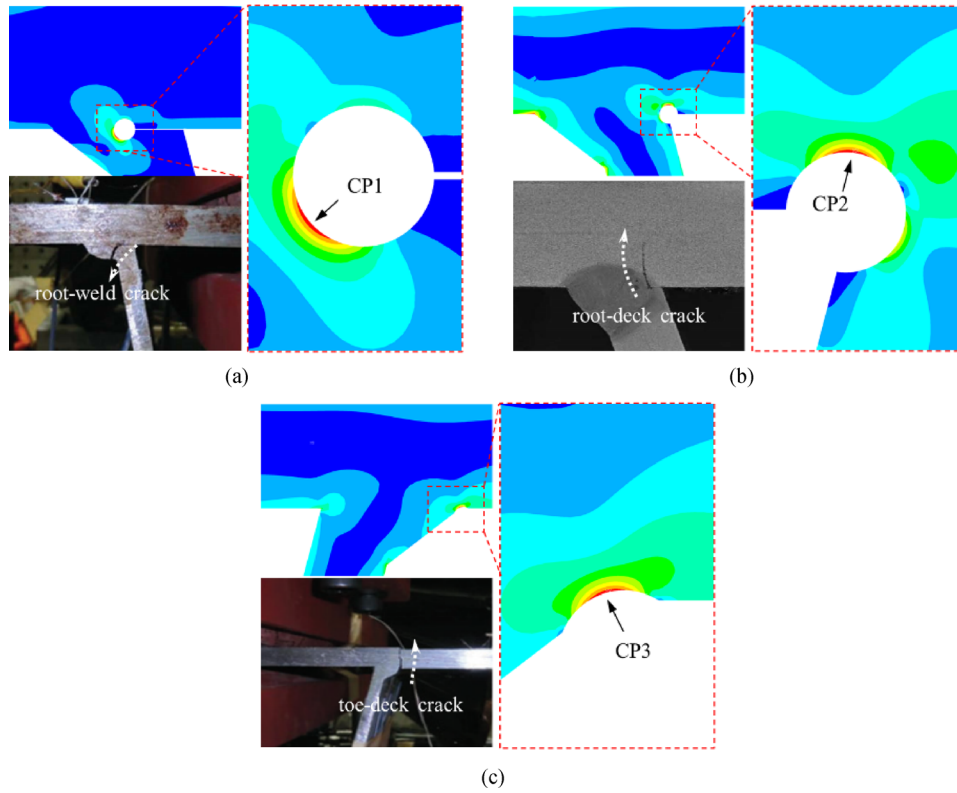
Fig. 10 Notch stress concentration positions obtained in this study. (a) Concentration position related to root–toe crack (CP1); (b) concentration position related to root–deck crack (CP2); (c) concentration position related to toe–deck crack (CP3).

combination of the variables to develop the formulas. Hence, we adopted multiple linear stepwise regression using a software named Statistical Product and Service Solutions (SPSS) developed by IBM. The linear regression functions with quadratic order and coupling terms are fitted using the values of K_f calculated from FEA, as expressed by Eq. (3).

$$K_f^{CPi} = \sum_{k=1}^{28} c_k^{CPi} \cdot f_k(X_1, X_2, X_3, X_4, X_5, X_6),\qquad (3)$$

where $i = 1$, 2, and 3, e.g., K_f^{CPi} represents K_f in CP1; $X_1 = 1 - t_p/t_r$; $X_2 = t_r/10$; $X_3 = l_{w,d}/t_r$; $X_4 = l_{w,r}/t_r$; $X_5 = 2\theta/180°$; $X_6 = t_d/t_r$; c_k^{CPi} are the coefficients obtained by the regression analysis. Since six normalized variables (X_1, X_2, X_3, X_4, X_5, and X_6), their squares, each combination of two variables, and an additional constant term (i.e., c_k^{CPi}) are used, a total of 28 terms are involved in the regression functions. Among the 28 terms, some may be dominant; however, the effect of a part of the terms on K_f could be neglected, as illustrated in the parametric analysis. To simplify the regression functions, the variables were automatically reduced during the regression process [11]. That is, only the variables that meet the conditions of significance and importance filter are considered in the regression functions.

The detailed stepwise regression analysis results are given in Appendix A. The coefficients of the regression formula for K_f^{CP1}, K_f^{CP2}, and K_f^{CP3} are listed in Table 2. The coefficients could be related to their influence on the dependent variable (i.e., K_f). Table 2 shows that some of the coefficients are set to zero, indicating that the influence of the corresponding terms on K_f could be neglected. Additionally, the absolute value of the coefficient quantifies the influence of the corresponding term, whereas the negative sign only represents the variation trend of K_f. Taking the coefficient of $X1$ (i.e., $1 - t_p/t_r$) for instance, the value of c_k^{CP1} is -12.861. The negative sign indicates that K_f^{CP1} decreases as X_1 increases, and the absolute value indicates the considerable effect of X_1 on K_f^{CP1} that are consistent with the results plotted in Fig. 11.

Figure 14 compares the values of K_f^{CP1}, K_f^{CP2}, and K_f^{CP3} calculated by Eq. (3) and the values obtained by FEA. All the correlation coefficients (R^2) are close to 1.0, indicating that the proposed empirical formulas could provide good predictions of K_f^{CP1}, K_f^{CP2}, and K_f^{CP3}.

K_f could also be predicted using the Deep Neural Network (DNN) method, as reported in [11,23]. Compared with the proposed regression formulas, the DNN method can handle all load cases and give all results once. Meanwhile, uncertainties could be automatically
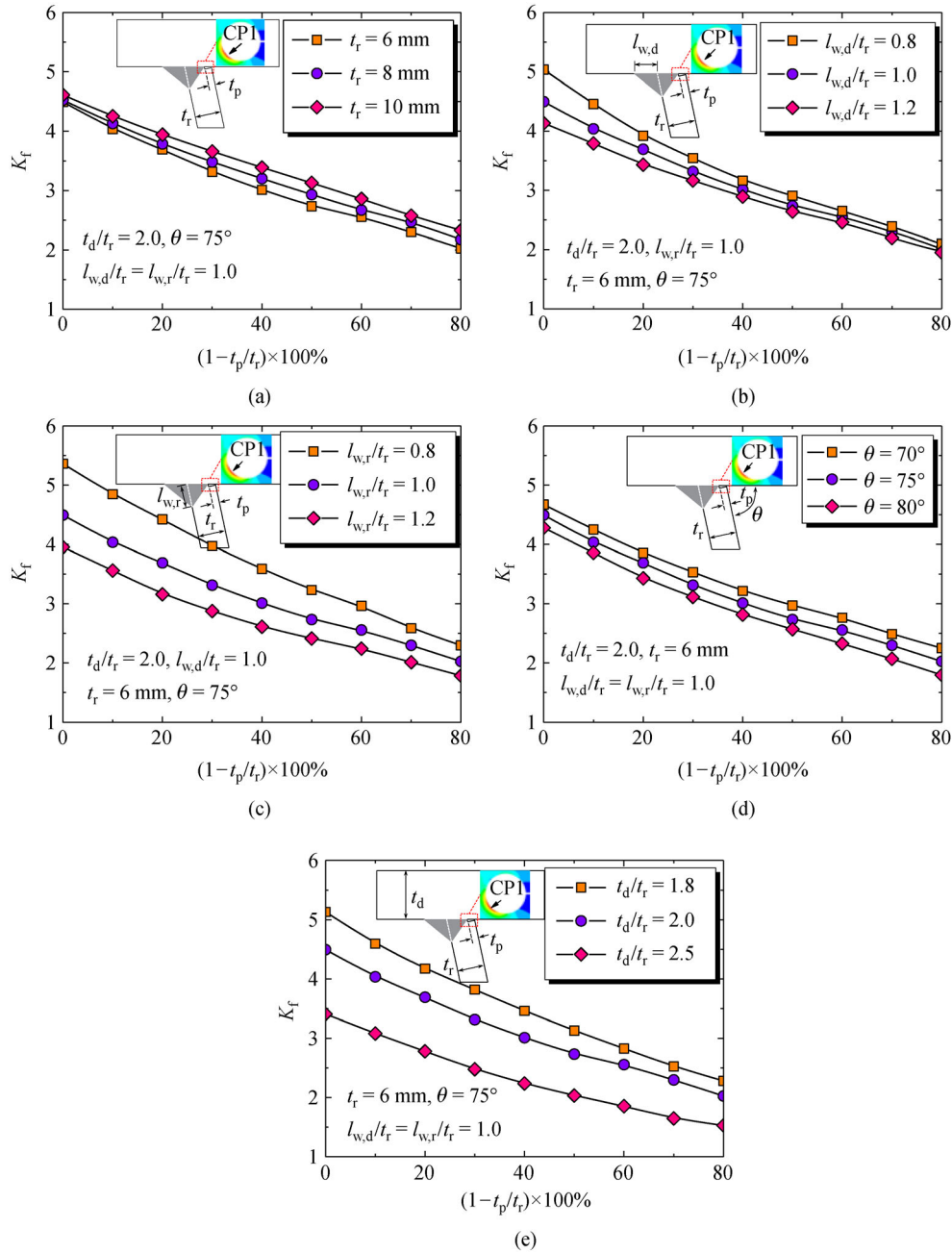
Fig. 11 Variation of effective notch stress concentration factor (K_f) at CP1 of weld root. (a) Effect of the weld penetration rate ($1 - t_p/t_r$) and rib thickness (t_r); (b) effect of the weld penetration rate ($1 - t_p/t_r$) and relative weld leg length in the deck ($l_{w,d}/t_r$); (c) effect of the weld penetration rate ($1 - t_p/t_r$) and relative weld leg length in the rib ($l_{w,r}/t_r$); (d) effect of the weld penetration rate ($1 - t_p/t_r$) and the angle between the deck and the rib (θ); (e) effect of the weld penetration rate ($1 - t_p/t_r$) and relative deck thickness (t_d/t_r).

accounted for due to the advantage of the DNN method. Further work is needed to employ the DNN method in predicting K_f.

5.2 Validation of the proposed formula

To further validate the reliability of the proposed formulas

for predicting K_f, we adopted additional data for $l_{w,d}/t_r = 0.6$, $l_{w,r}/t_r = 1.5$, $t_r = 7$ mm, and $\theta = 60°$, which were not considered in the regression analysis. The results are plotted in Fig. 15. We observed that the estimated values of K_f are in good agreement with the numerical results obtained by FEA. This demonstrates that the proposed formulas could be adopted for determining K_f in rib–deck welds.
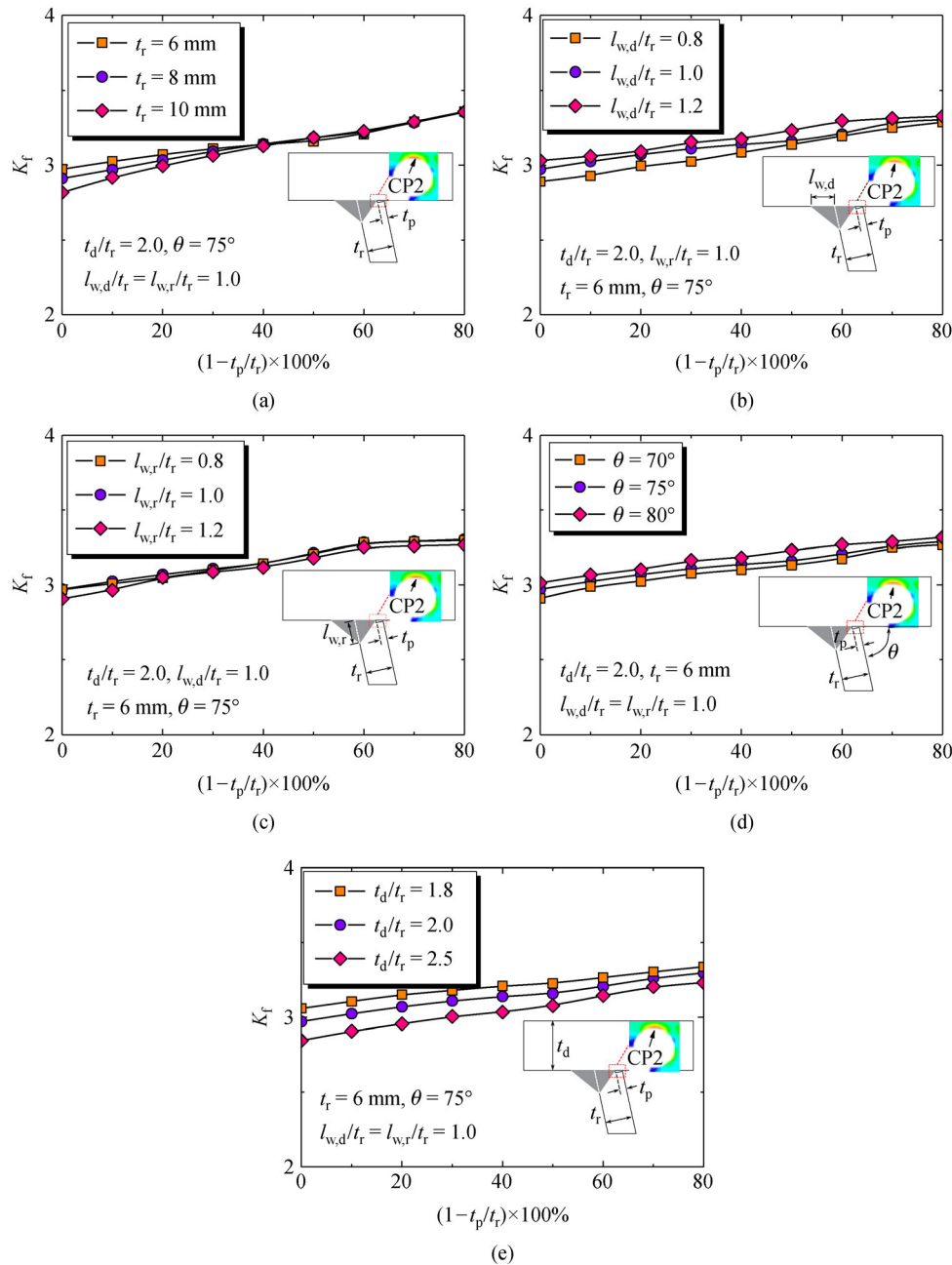
Fig. 12 Variation of K_f at CP2 of weld root. (a) Effect of the weld penetration rate $(1 - t_p/t_r)$ and t_r; (b) effect of the weld penetration rate $(1 - t_p/t_r)$ and $l_{w,d}/t_r$; (c) effect of the weld penetration rate $(1 - t_p/t_r)$ and $l_{w,r}/t_r$; (d) effect of the weld penetration rate $(1 - t_p/t_r)$ and θ; (e) effect of the weld penetration rate $(1 - t_p/t_r)$ and t_d/t_r.

6 Case study

Once the crack type is determined, K_f at the crack initiation position (i.e., the objective stress concentration position) could be quickly determined using Eq. (3). Then, the nominal stress-based fatigue data could be converted to the notch stress system, subsequently evaluated using the notch stress S–N curves. In this study, one example is presented to show the application of the proposed formulas for K_f.

6.1 Review of the fatigue test

Fatigue testing data of nine full-scale rib–deck welded specimens were considered [24]. The nine specimens were divided into three equal groups according to t_d (i.e., 14, 16, and 18 mm). All specimens had the same t_r of 8 mm and a penetration rate of 80%. The geometric parameters of the rib–deck weld are plotted in Fig. 16(a). For other geometric sizes of the specimen, please refer to Ref. [24]. Figure 16(b) shows the experimental diagram of the
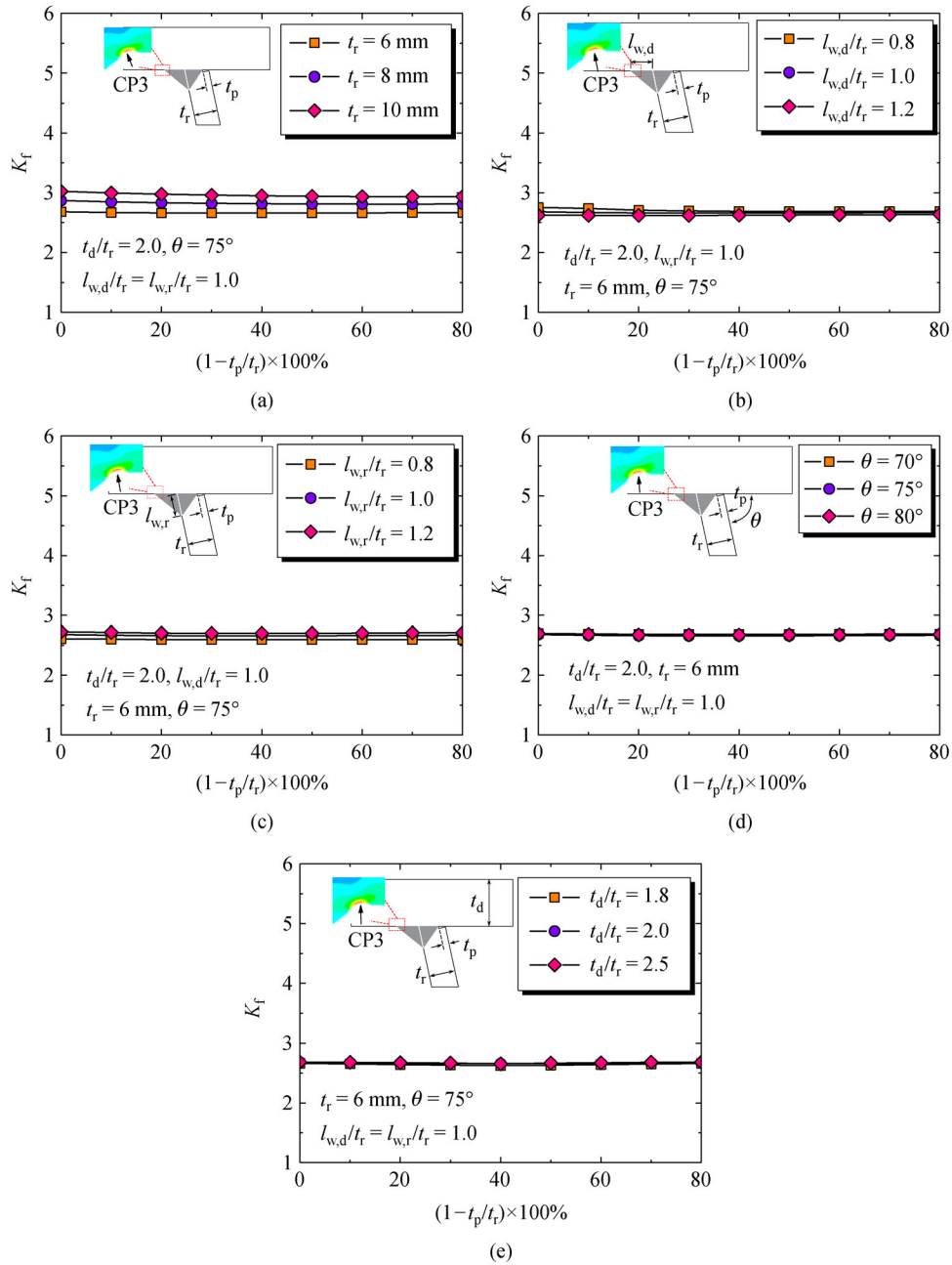
Fig. 13 Variation of K_f at CP3 of weld toe. (a) Effect of the weld penetration rate $(1 - t_p/t_r)$ and t_r; (b) effect of the weld penetration rate $(1 - t_p/t_r)$ and $l_{w,d}/t_r$; (c) effect of the weld penetration rate $(1 - t_p/t_r)$ and $l_{w,r}/t_r$; (d) effect of the weld penetration rate $(1 - t_p/t_r)$ and θ; (e) effect of the weld penetration rate $(1 - t_p/t_r)$ and t_d/t_r.

rib–deck welded specimens. The loading force was equally distributed by the distribution beam on the deck plate surface. Thus, the bending moment between the two loading positions was consistent. When a fatigue crack penetrated the deck plate, the specimen was considered failed, and the experiment was terminated. The definition of failure here is similar to that proposed by IIW [7]. Hence, the S–N curves recommended by IIW could be employed in evaluating fatigue testing data.

6.2 Application of the proposed formula

In the fatigue test, all the fatigue cracks initiated at the weld toe and propagated along the thickness of the deck plate, as shown in Fig. 17. Hence, K_f in the weld toe (i.e., K_f in CP3) needs to be determined. We developed FEMs to simulate 14, 16, and 18 mm thick specimens using the same modeling method discussed in Section 2 to determine the values of K_f. Furthermore, the proposed formula (Eq. (3)),

Table 2 Coefficients for the regression formula of K_f^{CP1}, K_f^{CP2}, and K_f^{CP3}

k	f_k	c_k^{CP1}	c_k^{CP2}	c_k^{CP3}	k	f_k	c_k^{CP1}	c_k^{CP2}	c_k^{CP3}
1	1	11.167	3.824	2.367	15	X_1X_3	2.159	−0.216	0.077
2	X_1	−12.861	0.000	0.000	16	X_1X_4	2.960	0.000	0.000
3	X_2	0.000	0.000	0.000	17	X_1X_5	0.000	0.000	0.000
4	X_3	0.000	0.000	0.000	18	X_1X_6	1.543	0.182	0.000
5	X_4	0.000	0.000	0.000	19	X_2X_3	0.000	0.000	0.000
6	X_5	0.000	0.000	0.000	20	X_2X_4	0.000	−0.320	0.873
7	X_6	0.000	−0.801	0.000	21	X_2X_5	0.000	0.000	0.000
8	X_1^2	1.363	−0.085	0.114	22	X_2X_6	0.177	0.000	0.000
9	X_2^2	0.000	0.000	0.000	23	X_3X_4	0.000	0.791	−0.259
10	X_3^2	0.000	−0.229	0.000	24	X_3X_5	0.000	0.000	0.000
11	X_4^2	1.989	−0.334	0.000	25	X_3X_6	−0.919	0.000	0.024
12	X_5^2	−2.245	0.353	0.000	26	X_4X_5	0.000	0.000	0.000
13	X_6^2	0.526	0.117	0.000	27	X_4X_6	−3.785	0.000	0.000
14	X_1X_2	0.792	0.578	−0.295	28	X_5X_6	0.000	0.000	0.000
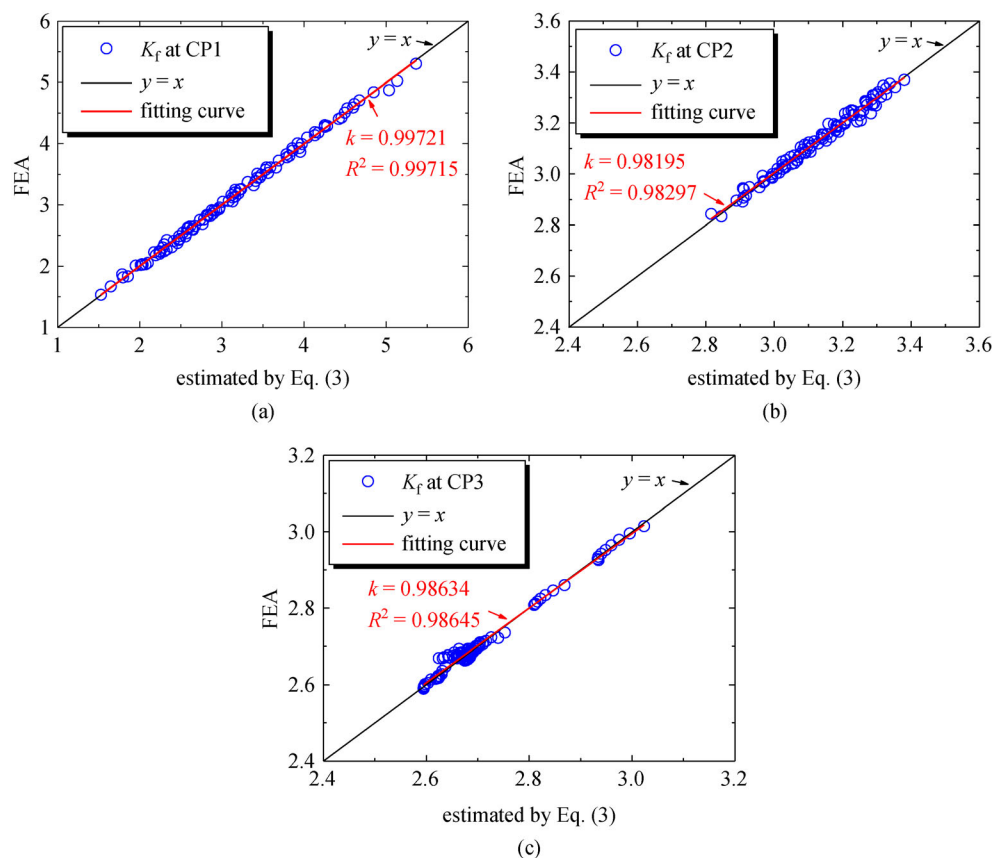
Fig. 14 Comparison of FEA and estimated results. (a) K_f at CP1; (b) K_f at CP2; (c) K_f at CP3.

as well as the coefficients listed in Table 2, was also adopted to predict the values of K_f. The FEA and estimated results are compared in Table 3, and they are in good agreement, with a maximum discrepancy of 2.91%.

6.3 Fatigue data in the notch stress system

The estimated values of K_f were applied, and then, the nominal stress-based fatigue data were converted to the
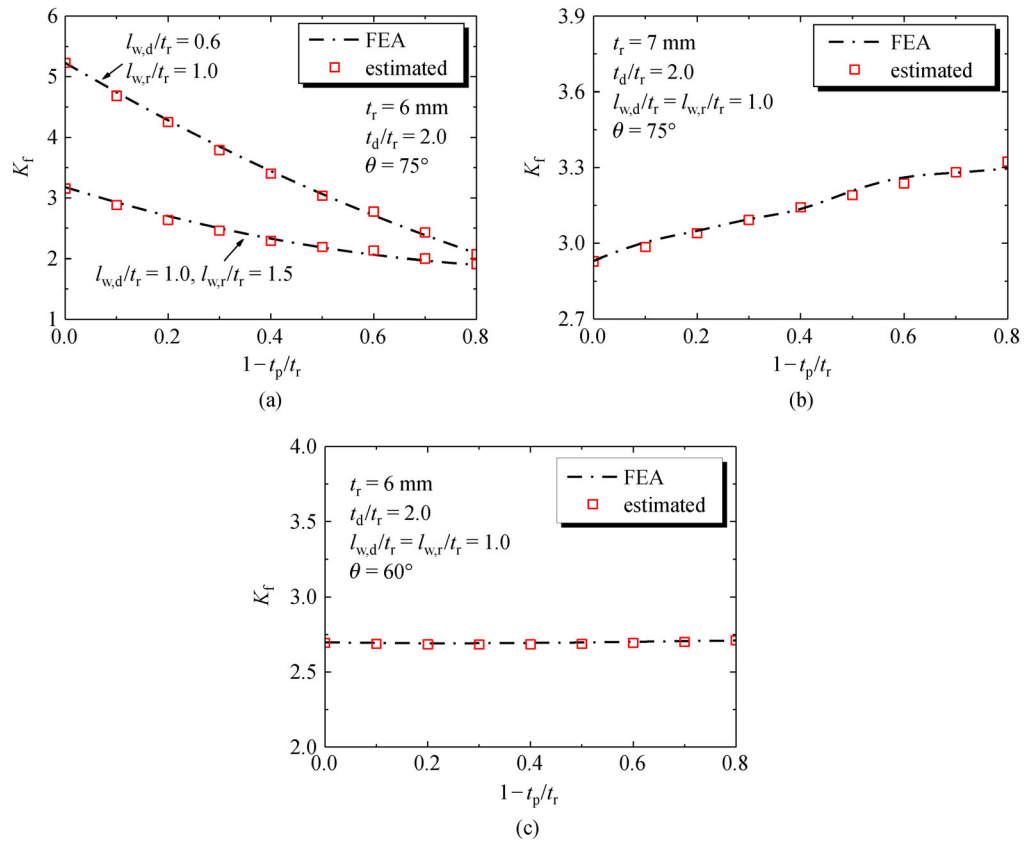
Fig. 15   Validation of the proposed formula using additional data. (a) K_f at CP1; (b) K_f at CP2; (c) K_f at CP3.
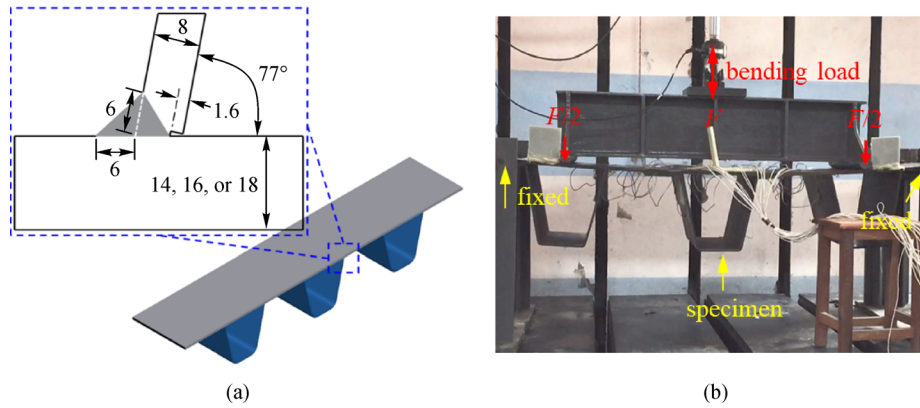

Fig. 16   Illustration of the fatigue test. (a) Geometry of full and 80% penetrated specimens; (b) bending loading mode.

Table 3   Comparison of FEA and estimated values of K_f

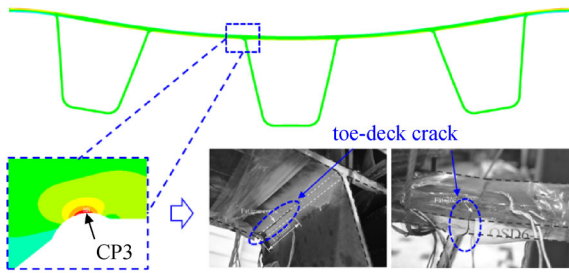| deck plate thickness (mm)	FEA, K_{f1}	estimated, K_{f2}	$(K_{f1} - K_{f2}) / K_{f2} \times 100\%$
14	2.681	2.707	−0.96%
16	2.759	2.711	1.77%
18	2.795	2.716	2.91%

Fig. 17 Notch stress concentration and fatigue cracking of OSD series.

effective notch stress-based fatigue data, as plotted in Fig. 18. The FAT class S–N curves are also included in the figure. All data points fall above the fatigue design curve of FAT225 in the IIW fatigue design recommendations [7]. The data points could also satisfy the S–N curves of FAT325 and FAT425. It implies that the fatigue design curve of FAT225 in the IIW fatigue design recommendations is conservative for the fatigue design of rib–deck welds possibly subjected to toe–deck cracking.
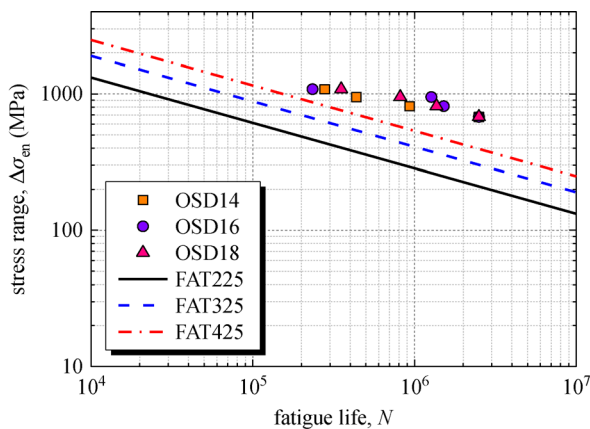

Fig. 18 Fatigue data in the notch stress system.

7 Conclusions

We performed a parametric analysis to investigate the effect of geometric parameters on the effective notch stress concentration factors (K_f) in rib–deck welds. We also performed regression analysis to develop empirical formulas for predicting K_f in rib–deck welds. A case study is presented to show the application of the proposed formulas. The following conclusions can be drawn.

1) We propose a modeling method for investigating the effective notch stress in rib–deck welds. The number of elements in the 360° arc should be no less than 26. The nominal stress point close to the weld toe or root should be 30 or 20 mm away from the weld toe or root, respectively.

2) Based on the parametric analysis results, we propose empirical formulas for predicting K_f in rib–deck welds.

The proposed formulas cover K_f for three types of fatigue-cracking modes. The correlation coefficients between the FEA and estimated results are close to 1.0, showing good agreement between the results.

3) A case study was conducted to exemplify the application of the proposed formulas. A maximum discrepancy of 2.91% between the FEA and estimated values of K_f confirms the reliability of the proposed formulas. FAT225 recommended by IIW seems conservative for evaluating the fatigue data of rib–deck welds. Further research is needed to develop the optimal notch stress-based S–N curves for rib–deck welds.

Appendix

Appendix A

The detailed stepwise regression analysis results of K_f^{CP1}, K_f^{CP2}, and K_f^{CP3} are listed in Tables A1, A2, and A3, respectively. To develop the optimal regression formula for K_f^{CP1}, 16 trial regression models were adopted. Similarly, 13 trial regression models were adopted for K_f^{CP2} and six models for K_f^{CP3}. The more independent variables the regression equation contains, the larger the correlation coefficients (R^2), the smaller the standard error of estimate, and the better the simulation effect. In this study, the final correlation coefficients (R^2) for K_f^{CP1}, K_f^{CP2}, and K_f^{CP3} were 0.997, 0.981, and 0.986, respectively.

Table A1 Stepwise regression analysis results of K_f^{CP1}

model	predictor variables	R^2	standard error of estimate
1	X_0, X_1X_6	0.832	0.35968972
2	X_0, X_1X_6, X_4X_6	0.930	0.23125343
3	$X_0, X_1X_6, X_4X_6, X_1X_5$	0.946	0.20322842
4	X_0, X_4X_6, X_1X_5	0.947	0.20242335
5	$X_0, X_4X_6, X_1X_5, X_3X_6$	0.961	0.17420706
6	$X_0, X_4X_6, X_1X_5, X_3X_6, X_1^2$	0.970	0.15196302
7	$X_0, X_4X_6, X_1X_5, X_3X_6, X_1^2, X_1X_2$	0.977	0.13208737
8	$X_0, X_4X_6, X_1X_5, X_3X_6, X_1^2, X_1X_2, X_1X_4$	0.980	0.12270214
9	$X_0, X_4X_6, X_1X_5, X_3X_6, X_1^2, X_1X_2, X_1X_4, X_1X_6$	0.985	0.10805856
10	$X_0, X_4X_6, X_1X_5, X_3X_6, X_1^2, X_1X_2, X_1X_4, X_1X_6, X_1$	0.989	0.09292036
11	$X_0, X_4X_6, X_1X_5, X_3X_6, X_1^2, X_1X_2, X_1X_4, X_1X_6, X_1, X_5^2$	0.992	0.07950012
12	$X_0, X_4X_6, X_3X_6, X_1^2, X_1X_2, X_1X_4, X_1X_6, X_1, X_5^2$	0.992	0.07909066
13	$X_0, X_4X_6, X_3X_6, X_1^2, X_1X_2, X_1X_4, X_1X_6, X_1, X_5^2, X_1X_3$	0.994	0.06530485

(Continued)

model	predictor variables	R^2	standard error of estimate
14	$X_0, X_4X_6, X_3X_6, X_1^2, X_1X_2, X_1X_4, X_1X_6, X_1, X_5^2, X_1X_3, X_2X_6$	0.995	0.06159826
15	$X_0, X_4X_6, X_3X_6, X_1^2, X_1X_2, X_1X_4, X_1X_6, X_1, X_5^2, X_1X_3, X_2X_6, X_6^2$	0.995	0.05886461
16	$X_0, X_4X_6, X_3X_6, X_1^2, X_1X_2, X_1X_4, X_1X_6, X_1, X_5^2, X_1X_3, X_2X_6, X_6^2, X_4^2$	0.997	0.04973409

Table A2   Stepwise regression analysis results of K_f^{CP2}

model	predictor variables	R^2	standard error of estimate
1	X_0, X_1X_3	0.856	0.04981720
2	X_0, X_1X_3, X_6	0.920	0.03700029
3	X_0, X_1X_3, X_6, X_5^2	0.931	0.03432015
4	$X_0, X_1X_3, X_6, X_5^2, X_2X_4$	0.939	0.03247062
5	$X_0, X_1X_3, X_6, X_5^2, X_2X_4, X_1X_2$	0.953	0.02850526
6	$X_0, X_1X_3, X_6, X_5^2, X_2X_4, X_1X_2, X_3X_4$	0.969	0.02319788
7	$X_0, X_6, X_5^2, X_2X_4, X_1X_2, X_3X_4$	0.969	0.02321962
8	$X_0, X_6, X_5^2, X_2X_4, X_1X_2, X_3X_4, X_4^2$	0.971	0.02241161
9	$X_0, X_6, X_5^2, X_2X_4, X_1X_2, X_3X_4, X_4^2, X_1X_6$	0.974	0.02118114
10	$X_0, X_6, X_5^2, X_2X_4, X_1X_2, X_3X_4, X_4^2, X_1X_6, X_1X_3$	0.977	0.01988373
11	$X_0, X_6, X_5^2, X_2X_4, X_1X_2, X_3X_4, X_4^2, X_1X_6, X_1X_3, X_6^2$	0.979	0.01901173
12	$X_0, X_6, X_5^2, X_2X_4, X_1X_2, X_3X_4, X_4^2, X_1X_6, X_1X_3, X_6^2, X_1^2$	0.980	0.01836800
13	$X_0, X_6, X_5^2, X_2X_4, X_1X_2, X_3X_4, X_4^2, X_1X_6, X_1X_3, X_6^2, X_1^2, X_3^2$	0.981	0.01806100

Table A3   Stepwise regression analysis results of K_f^{CP3}

model	predictor variables	R^2	standard error of estimate
1	X_0, X_2X_4	0.918	0.03051650
2	X_0, X_2X_4, X_3X_4	0.967	0.01940469
3	$X_0, X_2X_4, X_3X_4, X_1X_2$	0.975	0.01685447
4	$X_0, X_2X_4, X_3X_4, X_1X_2, X_1^2$	0.982	0.01423178
5	$X_0, X_2X_4, X_3X_4, X_1X_2, X_1^2, X_3X_6$	0.984	0.01355348
6	$X_0, X_2X_4, X_3X_4, X_1X_2, X_1^2, X_3X_6, X_1X_3$	0.986	0.01291298

References

1. Cheng B, Ye X H, Cao X E, Mbako D D, Cao Y S. Experimental study on fatigue failure of rib-to-deck welded connections in orthotropic steel bridge decks. International Journal of Fatigue, 2017, 103: 157–167

2. Ya S, Yamada K, Ishikawa T. Fatigue evaluation of rib-to-deck welded joints of orthotropic steel bridge deck. Journal of Bridge Engineering, 2011, 16(4): 492–499

3. Li M, Suzuki Y, Hashimoto K, Sugiura K. Experimental study on fatigue resistance of rib-to-deck joint in orthotropic steel bridge deck. Journal of Bridge Engineering, 2018, 23(2): 04017128

4. Luo P J, Zhang Q H, Bao Y. Predicting weld root notch stress intensity factors for rib-to-deck welded joint under deck loading modes. International Journal of Fatigue, 2019, 128: 105212

5. Fu Z Q, Ji B H, Zhang C Y, Wang Q D. Fatigue performance of roof and U-rib weld of orthotropic steel bridge deck with different penetration rates. Journal of Bridge Engineering, 2017, 22(6): 04017016

6. Dung C V, Sasaki E, Tajima K, Suzuki T. Investigations on the effect of weld penetration on fatigue strength of rib-to-deck welded joints in orthotropic steel decks. International Journal of Steel Structures, 2015, 15(2): 299–310

7. Hobbacher A. Recommendations for Fatigue Design of Welded Joints and Components. Berlin: Springer International Publishing, 2015.

8. Radaj D. Design and Analysis of Fatigue Resistant Welded Structures. Cambridge: Woodhead Publishing Series in Welding and Other Joining Technologies, 1990

9. Neuber H. On the consideration of the stress concentration in strength calculations. Design in Machinery and Equipment Construction, 1968, 20(7): 245–251 (in Deutsch)

10. Köttgen V B, Olivier R, Seeger T. Fatigue analysis of welded connections based on local stresses. Document IIW XIII–1408–91. Cambridge: Abington Publishing, 1992

11. Oswald M, Mayr C, Rother K. Determination of notch factors for welded cruciform joints based on numerical analysis and metamodeling. Welding in the World, 2019, 63(5): 1339–1354

12. Yung J L, Lawrence F V. Analytical and graphical aids for the fatigue design of weldments. Fatigue & Fracture of Engineering Materials & Structures, 1985, 8(3): 223–241

13. Radaj D, Zhang S. Multiparameter design optimization in respect of stress concentrations. In: Springer-Verlag (ed) engineering optimisation in design processes. Berlin: Springer, 1991, 181–189

14. Ushirokawa O, Nakayama E. Stress Concentration Factor at Welded Joints. Ishikawajima-Harima Gihou, 1983, 23: 351–355

15. Terán G, Albiter A, Cuamatzi-Meléndez R. Parametric evaluation of the stress concentration factors in T-butt welded connections. Engineering Structures, 2013, 56: 1484–1495

16. Brennan F P, Peleties P, Hellier A K. Predicting weld toe stress concentration factors for T and skewed T-joint plate connections. International Journal of Fatigue, 2000, 22(7): 573–584

17. Pachoud A J, Manso P A, Schleiss A J. New parametric equations to estimate notch stress concentration factors at butt welded joints modeling the weld profile with splines. Engineering Failure

Analysis, 2017, 72: 11–24

18. Wang Q D, Ji B H, Fu Z Q, Yao Y. Effective notch stress approach-based fatigue evaluation of rib-to-deck welds including pavement surfacing effects. International Journal of Steel Structures, 2020, 20(1): 272–286

19. Wang Q D, Ji B H, Fu Z Q, Ye Z. Evaluation of crack propagation and fatigue strength of rib-to-deck welds based on effective notch stress method. Construction & Building Materials, 2019, 201: 51–61

20. Park W, Miki C. Fatigue assessment of large-size welded joints based on the effective notch stress approach. International Journal of Fatigue, 2008, 30(9): 1556–1568

21. Horgan C O, Knowles J K. Recent developments concerning Saint-Venant's principle. Advances in Applied Mechanics, 1983, 23: 179–269

22. Yamada K, Ya S. Plate bending fatigue tests for root crack of trough rib of orthotropic steel deck. Journal of Structural Engineering JSCE, 2008, 54: 675–684 (in Japanese)

23. Samaniego E, Anitescu C, Goswami S, Nguyen-Thanh V M, Guo H, Hamdia K, Zhuang X, Rabczuk T. An energy approach to the solution of partial differential equations in computational mechanics via machine learning: Concepts, implementation and applications. Computer Methods in Applied Mechanics and Engineering, 2020, 362: 112790

24. Ding Y L, Song Y S, Cao B Y, Wang G X, Li A Q. Full-range S-N fatigue-life evaluation method for welded bridge structures considering hot-spot and welding residual stress. Journal of Bridge Engineering, 2016, 21(12): 04016096